EFDA–JET–CP(08)02/24

R.A. Pitts, G. Arnoux, M. Beurskens, T. Eich, W. Fundamenski, A. Huber, A. Loarte, J. Marki, M.F. Stamp, S. Brezinsek, H.G. Esser, B. Gulejova, S. Jachmich, A. Kreter, E. de la Luna, G.F. Matthews, V. Philipps, E. Solano and JET EFDA contributors

The Impact of Large ELMs on JET

The Impact of Large ELMs on JET

R.A. Pitts[1], G. Arnoux[2], M. Beurskens[3], T. Eich[3], W. Fundamenski[2], A. Huber[4], A. Loarte[5] J. Marki[5], M.F. Stamp[2], S. Brezinsek[4], H.G. Esser[4], B. Gulejova[1], S. Jachmich[6], A. Kreter[4], E. de la Luna[5], G. F. Matthews[2], V. Philipps[4], E. Solano[7] and JET EFDA contributors*

JET-EFDA, Culham Science Centre, OX14 3DB, Abingdon, UK

[1]CRPP-EPFL, Association EURATOM-Confédération Suisse, CH-1015 Lausanne, Switzerland
[2]EURATOM-UKAEA Fusion Association, Culham Science Centre, OX14 3DB, Abingdon, OXON, UK
[3]Max-Planck-Institut für Plasmaphysik, IPP-EURATOM Association, D-85748 Garching, Germany
[4]Institut für Energieforschung-Plasmaphysik, Forschungszentrum Jülich, Association EURATOM-FZJ, Germany
[5]ITER Organization, CEA-Cadarache Centre, 13108 Saint Paul les Durance, France
[6]LPP, ERM/KMS, Association Euratom-Belgian State, B-1000, Brussels, Belgium
[7]Associacion Euratom/CIEMAT para Fusion, Madrid, Spain
** See annex of M.L. Watkins et al, "Overview of JET Results ",*
(Proc. 21 st IAEA Fusion Energy Conference, Chengdu, China (2006)).

Preprint of Paper to be submitted for publication in Proceedings of the
18th Plasma Surface Interactions in Controlled Fusion Devices, Toledo, Spain
(26th May 2008 - 30th May 2008)

ABSTRACT.

To ensure sufficient divertor target lifetime, the loss in plasma stored energy due to ELMs in ITER should be restricted to $\Delta W_{ELM} \sim 1$MJ. Only in JET, by virtue of its size, can such energies be approached. This contribution examines the impact of large ELMs in high current H – mode JET discharges with ITER – relevant pedestal characteristics and the carbon MarkIISRP and HD divertors. The ELMs provoke strong radiation losses, mostly confined to the inner divertor volume, which are generally $\sim 0.5\Delta W_{ELM}$, but which can reach $\sim 0.7\Delta W_{ELM}$ for the largest ΔW_{ELM}, indicating enhanced impurity release. Peak divertor target surface temperatures are too low for carbon sublimation, suggesting that thermal decomposition and/or ablation of thick co-deposited layers on the inner target may be occurring. The largest ELMs deposit on average ~10% of ΔW_{ELM} on main wall surfaces, an energy fraction which is well reproduced by a model of ELM filament parallel energy losses developed at JET.

1. INTRODUCTION

The ITER organisation has recently declared that in order to prevent unacceptable divertor target erosion due to Edge Localised Mode (ELM) transient heat loads, the loss in plasma stored energy at the ELM should be restricted to $\Delta W_{ELM} \sim 1$MJ [1]. For the projected ITER QDT = 10 baseline scenario this implies $\Delta W_{ELM}/W_{plasma} \sim 0.003$, smaller than any value currently found experimentally for (unmitigated) Type I ELMs. It is, however, considerably larger than can be accessed by today's devices, with the exception of JET which, by virtue of its size, can produce ELMs close to 1MJ. This contribution summarises the results of experiments at JET designed to study large ELMs and to characterise their impact on the divertor plasma and on first wall and divertor target surfaces.

2. EXPERIMENTAL

To access the highest possible ΔW_{ELM}, JET has been run at $I_p = 3.0$MA ($B_\varphi = 3.0$T) in a series of dedicated discharges with fixed plasma shape, progressively decreasing the gas fuelling, Γ_{gas}, from shot to shot. This produces a scan in ELM amplitude and frequency at high W_{plasma} (~8MJ) with the largest $\Delta W_{ELM} \sim 0.8 - 0.9$MJ being found at $\Gamma_{gas} = 0$, for which the plasma density reaches only ~0.4 of the Greenwald limit. The plasma shape in this recent experiment is very close to the diagnostic optimised configuration (DOC – L) used in the past for ELM studies on JET [2] and is a vertical target equilibrium with strike points on the lower, CFC vertical tiles of the MarkII HD divertor (Fig. 1). Tiles 3 and 7 are unique amongst the target set in having one of the CFC fibre weaves in the toroidal direction, restricting poloidal heat conduction and maximising the surface temperature increase for given heat load. With $\delta = 0.25$, $\kappa = 1.72$ and $q_{95} \sim 3.1$, the configuration is similar to the projected ITER baseline Hmode equilibrium [3].

A selection of key plasma parameters for one of the recent unfuelled H-modes are compiled in Fig. 2a-g. With ~20MW of NBI heating (Fig. 1b) and a small amount of ICRH (coupling efficiency is limited during large ELMs), the injected energy in these discharges is in the range 160-195 MJ.

Of this, ~90MJ is found on Tiles 3,7 (Fig. 1) in the ratio 2.9 – 3.5:1 in favour of the outer target, entirely consistent with earlier findings for ELM averaged energy asymmetries [4]. Total radiated energies in the range 70 – 90MJ provide reasonable global power balance across the discharge series. The largest ELMs are generally sporadic (Fig. 2a) and often compound, characterised by a sharp initial drop in W_{plasma} and followed by a phase of smaller ELMs (possibly Type III), during which stored energy leaks out on a slower timescale. Energy confinement (expressed in terms of the H_{98} (y,2) scaling (Fig. 2f)) generally remains above unity, implying that the compound phases do not signal a return to L-mode. In the pre-ELM phases, electron temperature and density at the H-mode pedestal top (Fig. 2d,e) are in the range 5-6 x 10^{19} m^{-3} and 2-2.5keV respectively, yielding neoclassical pedestal collisionalities $\upsilon_e^* = 0.03 - 0.06$ in the range expected on ITER [2] and $\Delta W_{ELM}/W_{ped} \sim 0.2$ for the largest ELMs. In general, large ELMs provoke only modest increases in line integral Z_{eff} (Fig. 2g), with the exception of isolated events (e.g. prolonged compound phases) during which confinement is degraded significantly.

3. ELM – INDUCED RADIATION

Thanks to a major upgrade of the JET bolometer camera diagnostic [5], a 10 – fold increase in time resolution compared with the previous system now permits measurement of the energy radiated per ELM on the 1 ms timescale. Figure 3a concentrates on a single large event with $\Delta W_{ELM} \sim 0.85$MJ, of which $\Delta E_{RAD} = 0.58$MJ is radiated within ~6ms of the pedestal crash ($\Delta W_{ELM}/\Delta E_{RAD} = 0.68$). By the end of the compound phase, a total of 1.29MJ of stored energy has been lost, of which 1.08 MJ (84%) has been radiated. The tomographic reconstruction shown in Fig. 3b, averaged over the ~ 4ms period of the main radiated power peak following the ELM crash (inversions on the 1 ms timescale are numerically difficult to produce) illustrates the localisation of the radiated power distribution to the inner divertor volume (similar to ELM resolved bolometric reconstructions first performed on ASDEX Upgrade [6]). This is very likely to be a consequence of two principal factors: (i) the ELMs are known to deposit their energy asymmetrically, very clearly favouring the inner divertor over the outer in the ratio 2:1 on JET [7] and (ii) the inner divertor is a region of strong net codeposition, with thick, deuterium rich carbon layers accumulating over any given operational campaign [8].

The single ELM case shown in Fig. 3 is included in Fig. 4 which provides the ΔE_{RAD} dependence on ΔW_{ELM} for all ELMs identified in the 3.0MA gas scan series (initial ELM crash only – subsequent radiative release during compound phases is not included). Although there is considerable scatter, the data are generally consistent with $\Delta E_{RAD} \sim 0.5 \Delta W_{ELM}$, except at the highest ΔW_{ELM} (of which Fig. 3 is an example), where there are indications for an enhanced effect (see also [9]).

These ELM induced radiation losses may be compared with those reported in [10] from the earlier DOC – L experiment in the MarkIISRP divertor (before the bolometer diagnostic upgrade), where $\Delta E_{RAD} \sim 0.25 \Delta W_{ELM}$ was observed for $\Delta W_{ELM} \leq 0.7$ MJ (similarly to Fig. 4), marking a sharp threshold beyond which radiation was considerably enhanced. In fact, the 5 values of ΔW_{ELM} were somewhat overestimated in [10] such that the threshold probably occurred at even lower ΔW_{ELM}. In

the absence of target surface temperature measurements, thermal sublimation was proposed as the mechanism for the apparently increased impurity release. Analysis of IR data obtained during these older experiments (the equivalent data in the more recent experiment is unfortunately lacking) has since become available and is compiled in Fig. 5, giving the peak surface temperature dependence on the corrected ΔW_{ELM} for a range of DOC-L discharges with varying Ip (but constant q_{95}), during which the largest $\Delta W_{ELM} \sim 0.7$MJ were also obtained at $I_p = 3.0$MA. The effect of surface layers can be seen in the abrupt rise of the baseline temperature on the inner target even at low ΔW_{ELM}. Maximum excursions of ~520ºC and ~550ºC are seen at the outer and inner targets respectively, pushing temperatures up to ~1130ºC at the outer target (where the higher inter-ELM heat fluxes drive the baseline temperature higher). Even though instrumental considerations could imply that the real temperature is somewhat higher, this correction is unlikely to exceed ~200ºC, so that the peak values cited above are still far short of what is required for radiation enhanced sublimation of graphite, which becomes effective in the region of 2200ºC and above in tokamaks [11].

The strong radiation asymmetry in favour of the inner divertor, which can reach as much as 5:1 (see [10]) is strongly suggestive that the deposited layers play a key role, especially since peak temperatures at the outer target are even higher than those observed at the inner (Fig. 5). Whilst it cannot be proven with the available data, the impurity release is likely a combination of layer thermal decomposition and ablation. The former is known to be operative in the JET inner divertor, having been deduced from spectroscopic measurements of strong C_2 and CD emission in ELMing H-mode discharges with strike points positioned on the horizontal base tiles (numbers 4,6 in Fig. 1) where soft a-C:H layers are formed by redeposition of carbon eroded from the vertical tiles [12]. Such a process is also offered in [13] as an explanation for the non-linear increase in the erosion measured in JET beyond a given ELM size using in-situ Quartz Micro Balance detectors (the inner divertor QMB may be seen in Fig. 1). A possible explanation for the enhanced radiation seen for $\Delta W_{ELM} > 0.7$MJ in Fig. 4 is layer ablation, perhaps accompanied by the release of macroscopic clusters. Both thermal decomposition and ablation provide a rich source of carbon which would radiate strongly depending on the efficiency with which the released particles penetrate the inner divertor plasma, itself changing rapidly on the timescale of the transient.

4. MAIN WALL ENERGY LOADS

Now seen in all tokamaks where they have been sought [14] and on a variety of diagnostics at JET [15-18], ELM filaments convecting plasma rapidly across the magnetic field in the Scrape-Off Layer (SOL) to main chamber surfaces are a concern for ITER [1]. A recent addition to the JET diagnostic set is a wide angle, main chamber viewing IR camera system which supplies some hitherto inaccessible data concerning first wall power loads [19]. Inspection of the IR images obtained in the relatively low triangularity discharges discussed here, reveals essentially no ELM interaction with the upper dump plates and none on the inner wall. By far the largest deposition occurs on the divertor targets, but there is a non – negligible interaction with the low field side bumper limiters,

of which there are 16 on JET of practically identical design.

For most of the pulses the camera was employed in full frame mode, viewing the full poloidal cross-section with 8.4 ms time resolution, by far insufficient to resolve the time variation of the ELM energy deposition. In one or two cases, a sub-array was used to increase time resolution (to 1.4 ms, still too slow to properly resolve the ELM temperature increase) on a spatial region covering one of the poloidal limiters in the FOV. Estimating a toroidal temperature profile (poloidally averaged) for all times on each of the 15 tiles comprising each bumper limiter and subsequently computing power fluxes, yields an accumulated energy per tile. Summing the energies from all tiles and further assuming that (i) all 16 limiters receive identical averaged heat fluxes and (ii) that only ELM filaments are capable of depositing heat on the limiters (i.e. no inter-ELM heat flux and negligible deposition during any compound ELM phases), provides a total wall energy deposition for each discharge. Figure 6 illustrates this process for the zero gas fuelling shot of Fig. 2, where the image slices to the right show the limiter in question in ambient IR (i.e. without plasma) and during a single ELM. In general, the strongest interaction occurs on tiles in the outside midplane vicinity (Tiles 11-13 in Fig. 6), reflecting the ELM filament power exhaust localisation (see also [18]). Temperature excursions on these tiles can be significant (Fig. 6b), but there is indeed little or no rise during the inter-ELM periods. The accumulated energy for the example in Fig. 6 amounts to ~1.5MJ, to be compared with a total stored energy loss of $\Sigma\Delta W_{ELM} \sim 12.7$MJ (Fig. 6c). Table 1 compiles the results of this analysis for all shots in the series for which main chamber IR data are available. The data show a clear trend for the ELM wall loading to increase with average ELM size, in qualitative agreement with a recent scaling based on interchange dynamics, which predicts a square root dependence of ELM radial speed on ELM size [20].

The ELM averaged wall loadings in Table 1 offer an ideal further opportunity to confront experiment with the parallel filament loss model that has been developed at JET [21] and successfully applied to a variety of experimental situations [15,21,22]. If pedestal plasma profiles are available and separatrix-wall gaps known, the model requires only a value for the cross-field ELM filament propagation speed, vr,ELM and an assumption for the point in space at which the filament originates [21]. Figure 7b illustrates the application of the model to pulse #70224, for which good (pre-ELM) pedestal profiles of T_e and n_e are available (Fig. 7a) from the new JET High Resolution Thomson Scattering (HRTS) diagnostic. This is not, unfortunately, the case for the other discharges in the gas scan series. Based on these profiles, the pedestal width (shaded area in Fig. 7a) is ~4 cm, with $T_{e,pedt0} \sim 1500$eV, $n_{e,pedt0} \sim 5 \times 10^{19}$ m^{-3} at the pedestal top, $T_{e,sep0} \sim 200$eV, $n_{e,sep0} \sim 1 \times 10^{19}$ m^{-3} at the separatrix and $T_{e,pedm0} \sim 800$ eV, $n_{e,pedm0} \sim 3 \times 10^{19}$ m^{-3} at the mid – pedestal radius. The latter is reference point often employed in the parallel loss model in the absence of any physics model describing precisely where the ELM filaments originate [21]. Regarding $v_{r,ELM}$, recourse can be made to a previous detailed study on JET which found vr,ELM in the range 0.45-0.75 kms^{-1} in the SOL for high power H-modes, giving an average value of 0.6kms^{-1}

For comparison with experiment, the parameter $W' = W/W_0$, the filament stored energy ($W = 3/2n(T_i + T_e)$), normalised to the initial value at the start of propagation is plotted in

Fig. 7b for filaments originating at the pedestal top, the mid-pedestal radius and at the separatrix (assuming $T_i = T_e$). An additional set of curves serves as a crude sensitivity study in which $v_{r,ELM}$ has been doubled to $1.2 kms^{-1}$. At 5cm beyond the separatrix (the nominal minimum midplane mapped distance to the limiter) and with $v_{r,ELM}$ = 0.6kms-1, W' = 9.4%, 3.7% and 34.9% for filaments beginning at the mid-pedestal, pedestal top and separatrix radius respectively. For $v_{r,ELM}$ = $1.2 kms^{-1}$, the equivalent values are W' = 21.5%, 10.2% and 54.7%. These should be compared with the experimental quantity in the last column of Table 1 which, for #70224, yields 8.8%. At the wall, a filament originating at the pedestal top thus deposits the same fraction of its initial energy content as one formed further out in the pedestal but travelling at half the speed. Experimental data do not appear consistent with events originating at the separatrix unless they are travelling much more slowly (to deposit 10% of its initial energy at the wall, a filament released at the separatrix in the profile of Fig. 7a would require $v_{r,ELM} = 0.18 kms^{-1}$).

CONCLUSIONS

If material damage to the ITER divertor targets is to be avoided, the maximum loss in plasma stored energy per ELM must be restricted to ΔW_{ELM} ~1MJ. Such values can already be approached in JET (e.g. ΔW_{ELM} ~0.9MJ) at high current, high input power and low or zero gas fuelling ($n_e \sim 0.4 n_{GW}$). In the divertor, large ELM impact provokes intense radiation losses, mostly confined to the inner divertor volume, with $\Delta E_{RAD}/\Delta W_{ELM}$ reaching as much as 0.7 and some indication of a threshold near $\Delta W_{ELM} \sim 0.7$MJ, below which $\Delta E_{RAD}/\Delta W_{ELM} \sim 0.5$ is more generally observed. The plasma Z_{eff} does not appear to be unduly perturbed by the ELM induced impurity release. Peak divertor target surface temperatures are far short of the requirements for carbon sublimation, suggesting that thermal decomposition and ablation of co – deposited carbon layers on the inner target is occurring. The filaments associated with large ELMs are observed to deposit on average ~10% of ΔW_{ELM} at the main chamber outboard limiters. This energy fraction is in good agreement with a model of parallel filament losses developed at JET. It is also very close to the loss fraction estimated previously for unmitigated Type I ELMs on ITER using the same model [22].

ACKNOWLEDGEMENTS

This work was conducted under the European Fusion Development Agreement and was supported in part by the Swiss National Science Foundation, EURATOM and the UK Engineering and Physical Sciences Research Council.

REFERENCES

[1]. A. Loarte *et al.,* "Power and particle fluxes at the plasma edge of ITER : Specifications and Physics Basis" to be presented at 22nd IAEA Fusion Energy Conference, Geneva, Switzerland (2008).

[2]. A. Loarte *et al.,* Phys. Plasmas **11** (2004) 2668

[3]. M. Shimada. *et al*., Nucl. Fusion **47** (2007) S1
[4]. R.A. Pitts *et al*., J. Nucl. Mater. **337-339** (2005) 146
[5]. A. Huber *et al*., J. Nucl. Mater. **363-365** (2007) 365
[6]. J.C. Fuchs *et al*., J. Nucl. Mater. **337-339** (2005) 756
[7]. T. Eich *et al*., J. Nucl. Mater. 363-365 (2007) 989
[8]. J.P. Coad *et al*., Nucl. Fusion **46** (2006) 350
[9]. A. Huber *et al*., this conference, paper P2-24
[10]. A. Loarte *et al*., Phys. Src. T128 (2007) 222
[11]. W. Eckstein and V. Philipps, in Physical Processes of the Interaction of Fusion Plasmas with Solids, edited by W. Hofer and J. Roth (Academic Press, San Diego, 1996)
[12]. S. Brezinsek *et al*., J. Nucl. Mater. **337-339** (2005) 1058
[13]. A. Kreter *et al*., this conference, paper I-3
[14]. A. Kirk *et al*., this conference, paper I-5
[15]. R.A. Pitts *et al*., Nucl. Fusion **46** (2006) 82
[16]. A. Alonso *et al*., this conference, paper P1-39
[17]. C. Silva et al., this conference, paper P1-25
[18]. M. Jakubowski *et al*., this conference, paper P1-24
[19]. E. Gauthier *et al*., J. Nucl. Mater. **363-365** (2007) 1026
[20]. O.E. Garcia *et al*., Phys. Plasmas **13** (2006) 082309
[21]. W. Fundamenski, R. A. Pitts, Plasma Phys. Control. Fusion **48** (2006) 109
[22]. W. Fundamenski, R. A. Pitts *et al*., J. Nucl. Mater. **363-365** (2007) 319
[23]. W. Fundamenski, W. Sailer, Plasma Phys. Control. Fusion **46** (2004) 233

Pulse	No. ELMs	$\Sigma\Delta W_{ELM}$ (MJ)	ΣE_{LIM} (MJ)	$\langle\Sigma\Delta W_{ELM}\rangle$ (MJ)	$\Sigma E_{LIM}/\Sigma\Delta W_{ELM}$ (%)
70221	133	29.7	1.49	0.224	5.3
70222	87	23.7	1.02	0.275	4.3
70223	50	18.0	0.85	0.360	4.7
70224	16	8.34	0.71	0.521	8.8
70225	30	14.9	1.37	0.497	9.2
70226	24	12.7	1.49	0.528	0.528

Table 1: Summary of ELM statistics for 6 pulses in the 3.0 MA gas scan. Note that pulses 70225,6 have $\Gamma_{gas} = 0$.

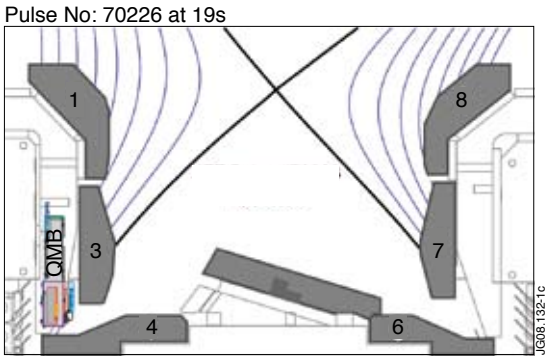

Figure 1: Mark IIHD divertor configuration with EFIT reconstruction.

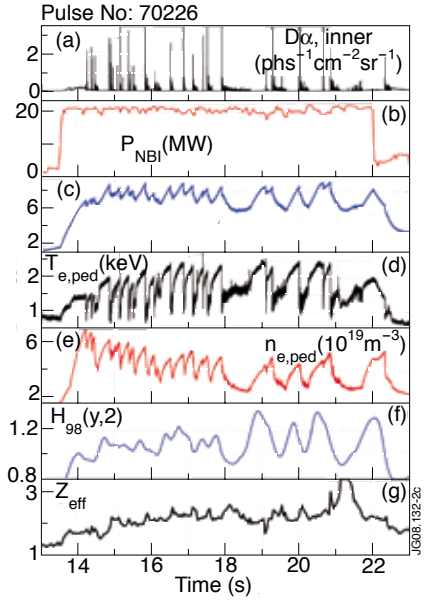

Figure 2: (a-g) Selected plasma signals for a 3.0MA H-mode discharge with $\Gamma_{gas} = 0$.

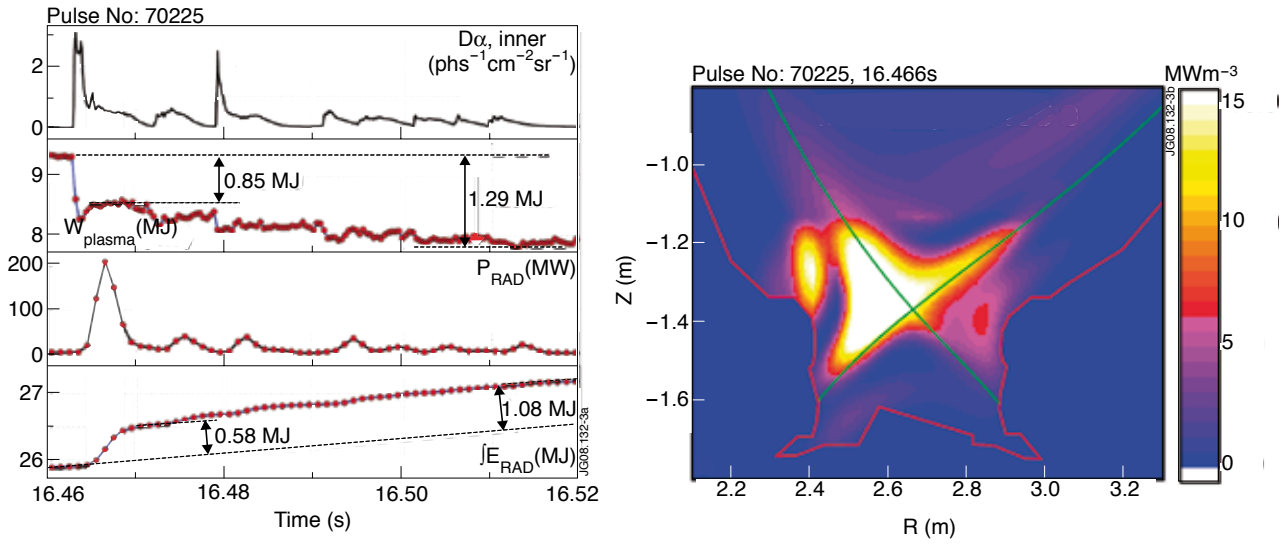

Figure 3: (a) Energy balance during a single large ELM. (b) Tomographic reconstruction of the ELM radiation distribution averaged over shaded region in (a).

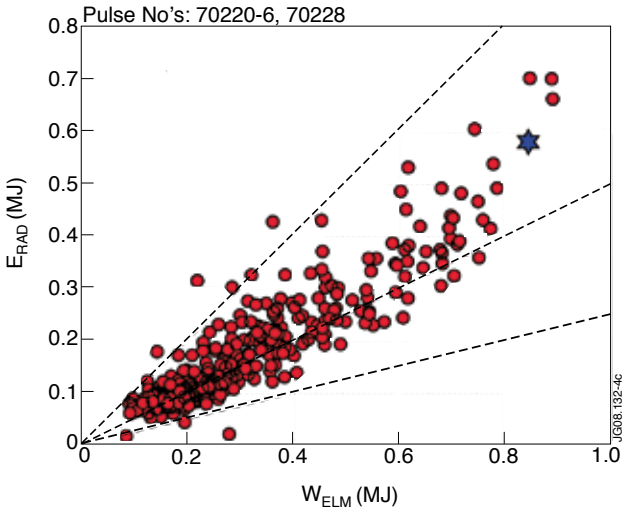

Figure 4: ΔE_{RAD} at the ΔW_{ELM} crash versus. ΔW_{ELM} for all ELMs found in the 3.0MA shot series. The symbol marks the ELM examined in detail in Fig. 2.

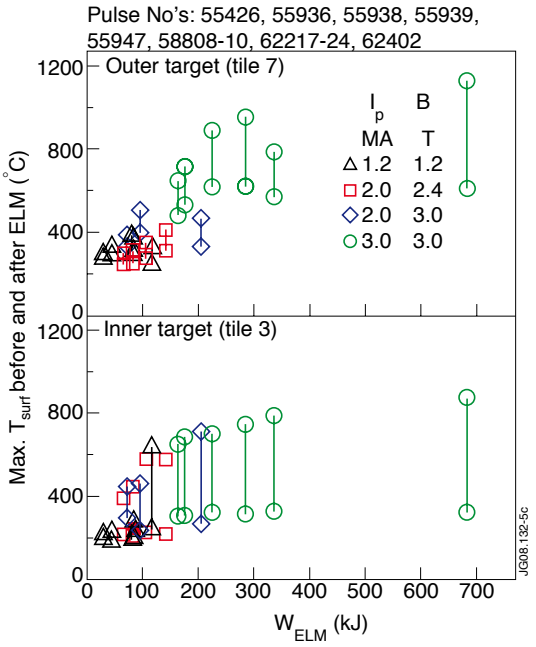

Figure 5: Peak divertor T_{surf} before and during ELMs. Results are obtained from coherent averaging of ELM groups near the end of the H-mode phase.

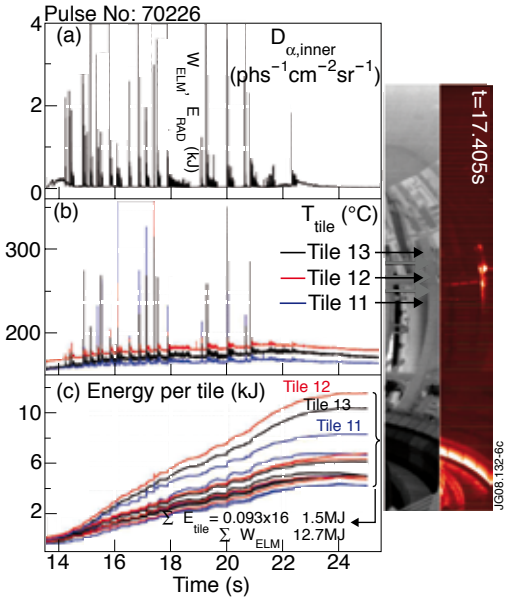

Figure 6: (b) Peak T_{surf} on three tiles of a single outboard limiter. (c) Accumulated energy for all 15 tiles. Selected ELM peaks on the inner divertor D_a in (a) are marked with the corresponding ΔW_{ELM} and DE_{RAD}.

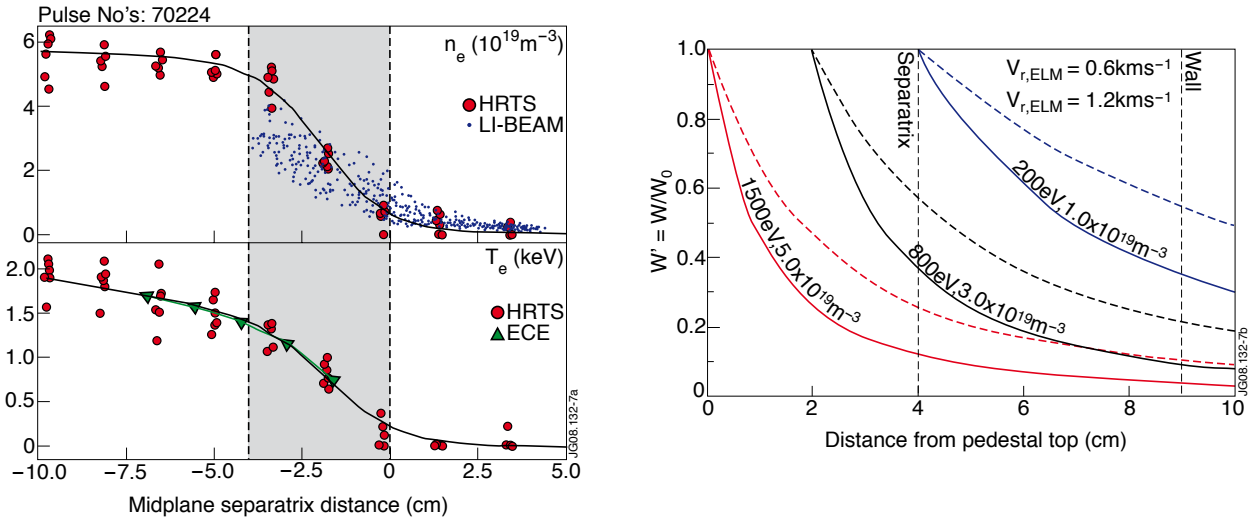

Figure 7: (a) Inter-ELM pedestal profiles. Solid lines are tanh fits to the HRTS data. (b) Model predictions for W'(r). Initial n_e,T_e at launch are marked.